

Interfacial Charge-transfer Doping of Metal Halide Perovskites for High Performance Photovoltaics

Nakita K. Noel,^{1,2*} Severin N. Habisreutinger,³ Alba Pellaroque,⁴ Federico Pulvirenti,⁵ Bernard Wenger,⁴ Fengyu Zhang,¹ Yen-Hung Lin,⁴ Obadiah G. Reid,^{3,6} Johannes Leisen,⁵ Yadong Zhang,⁵ Stephen Barlow,⁵ Seth R. Marder,⁵ Antoine Kahn,¹ Henry J. Snaith,⁴ Craig B. Arnold,² Barry P. Rand.^{1,7*}

¹ Department of Electrical Engineering, Princeton University, Princeton, NJ, 08544, USA

² Princeton Research Institute for the Science and Technology of Materials, Princeton University, Princeton, NJ, 08544, USA.

³ National Renewable Energy Laboratory, 15013 Denver West Parkway, Golden, Colorado, 80401, USA.

⁴ Clarendon Laboratory, Department of Physics, University of Oxford, Parks Road, Oxford, OX1 3PU, UK

⁵ School of Chemistry and Biochemistry and Center for Organic Photonics and Electronics, Georgia Institute of Technology, Atlanta, Georgia 30332-0400, USA.

⁶ Renewable and Sustainable Energy Institute, University of Colorado at Boulder, Boulder, CO 80309, USA

⁷ Andlinger Centre for Energy and the Environment, Princeton University, Princeton, NJ, 08544, USA

* Corresponding author: nnoel@princeton.edu; brand@princeton.edu

Supporting Information

Synthesis of Mo(dt)₃ Complexes:

The Mo(tfd-COCF₃)₃ and Mo(tfd-CO₂Me)₃ complexes were synthesised according to previously published methodologies.^{1,2}

Synthesis of Spiro-OMeTAD(TFSI)₂:

Spiro-OMeTAD(TFSI)₂ was synthesised using a modified version of the method previously described by Nguyen et al.³ Briefly, Spiro-OMeTAD was reacted with AgTFSI in a 1:2 molar ratio in dichloromethane and stirred for 24 h in the dark. The reaction was then diluted with toluene and a dark-green/black solid was obtained. The solid was isolated through filtration, and then washed with methanol, after which it was vacuum-dried for 24 h.

Carbon Nanotube Functionalisation:

This method is described in detail elsewhere.⁴ Briefly, rr-P3HT (3.0 mg, Rieke Metals Inc., weight-average molecular weight $M_w = 50\,000\text{ g mol}^{-1}$, and regioregularity = 95%) was dissolved in 5.00 mL of chlorobenzene and sonicated in a bath sonicator for 60 min. SWNTs (2.5 mg) were added, as purchased (Sigma-Aldrich (CG200)) to the P3HT solution and treated with an ultrasonic probe for 10 min. After sonication, 5 mL of chlorobenzene was added to improve the solubility of the polymer–nanotube hybrids. Subsequently, the dispersion was centrifuged for 8 min at 10 000g

to remove nonfunctionalized SWNTs and other carbonaceous particles. The precipitate was discarded while the supernatant was recovered. 10 mL of toluene was added then added to remove excess polymer. The mixture was then mildly heated for 60 min to induce aggregation of the functionalized SWNTs. The aggregates were then removed by centrifugation (4 min at 16 000g). The supernatant containing excess polymer was discarded, and the precipitate was recovered. The pellet consisted of 1.5–1.6 mg of polymer-wrapped nanotubes, which were dispersed in 6 mL of chloroform. Immediately prior to spin-coating, the chloroform dispersion was sonicated with an ultrasonic probe for 1 min at low intensity (~10% of amplitude) to break up clusters and bundles.

Fabrication of Planar Heterojunction Solar Cells:

Planar heterojunction solar cells were fabricated utilising previously published methods.⁴⁻⁶ Concisely, FTO-coated glass sheets ($15 \Omega\text{cm}^{-1}$ Hartford Glass) were etched with zinc powder and HCl (3M) to obtain the required electrode pattern. The sheets were then washed with soap (2% Hellmanex in water), deionised water, acetone, ethanol and isopropanol, and finally treated under oxygen plasma for 10 min to remove the last traces of organic residues. A compact layer of SnO_2 was then deposited on the glass using a modified version of the methodology presented by Anaraki et al.⁷ Briefly, $\text{SnCl}_4 \cdot 5\text{H}_2\text{O}$ was dissolved in isopropanol at a concentration of 0.05 M and stirred at room temperature for 30 min. The solution was then spin coated onto the substrates at 3000 rpm, after which the substrates were annealed at 180°C for 1 hour before being left to naturally cool down to room temperature. The substrates were then immersed into a chemical bath, which consisted of $\text{SnCl}_2 \cdot 2\text{H}_2\text{O}$ (Sigma-Aldrich) in deionised water (0.012 M), 20.7 mM urea (Sigma-Aldrich), 0.15 M HCl (Fisher Scientific) and $2.87 \mu\text{M}$ 3-mercaptopropionic acid (Sigma-Aldrich).

The substrates were kept in an oven at 70 °C for 180 min, after which they were sonicated in deionised water for 2 minutes. They were then washed with ethanol and annealed at 180 °C for 60 min. A 1.2 M solution of $\text{FA}_{0.85}\text{MA}_{0.15}\text{Pb}(\text{I}_{0.85}\text{Br}_{0.15})_3$ was prepared using a 4:1 vol.: vol. ratio of DMF: DMSO. The solution was spin coated onto the desired substrate at 1000 rpm for 10 s, followed by 6000 rpm for 35 s. 100 μL of anisole was dropped onto the substrate 35 s after the beginning of the spincoating. The films were then annealed at 100 °C for 60 min. After annealing, the substrates were allowed to cool to room temperature. $\text{Mo}(\text{tfd-COCF}_3)_3$ was dissolved in chlorobenzene at the desired concentration, and the solution was left stirring on a hotplate at 60 °C for 1 hr, after which it was cooled to room temperature. The $\text{Mo}(\text{tfd-COCF}_3)_3$ solution was then spin coated onto the perovskite surface at 2000 rpm for 45 s, after which the substrates were annealed at 100 °C for 10 min. After the substrates were cooled to room temperature, 50 μL of a dispersion of single-walled carbon nanotubes (SWNTs) in chloroform was deposited dynamically using drop-by-drop spin coating.⁴ For the deposition of the spiro-OMeTAD layer, 85 mg/mL of 2,20,7,70-tetrakis(N,N-di-pmethoxyphenyl-amine)9,9-spirobifluorene (Lumtec) was dissolved in chlorobenzene (Sigma-Aldrich), and 33 $\mu\text{L}/\text{ml}$ of 4-tert-butylpyridine (Sigma-Aldrich) was added. The solution was then deposited onto the desired substrate spin coating at 2000 rpm for 45 s. Finally, 80 nm thick gold electrodes were deposited under high vacuum (10^{-7}) in a thermal evaporator using a shadow mask.

Fabrication of Perovskite Films for Characterisation:

Perovskite films were deposited on glass, FTO, or ITO (for XPS/UPS measurements) using the method described above.

Current-Voltage Characterisation:

Solar cell performance was measured using a class AAB ABET sun 2000 solar simulator that was calibrated to give simulated AM 1.5 sunlight at an irradiance of 100 mW/cm^2 . The irradiance was calibrated using an NREL-calibrated KG5-filtered silicon reference cell. Current-voltage curves were recorded using a sourcemeter (Keithley 2400, USA). All solar cells were masked with a metal aperture that was used to define the active area of the devices, which in this case was 0.1 cm^2 . All devices with selective contacts were stored in a desiccator in the dark for 12 h before testing, while devices without selective contacts were tested immediately after fabrication. All devices were scanned without pre-biasing, at a speed of 0.15 V/s .

Optical Characterisation:

Absorption spectra were recorded on a Cary 5000 Uv-Vis spectrophotometer. Time-resolved PL measurements were acquired using a time-correlated single photon counting (TCSPC) setup (FluoTime 300 PicoQuant GmbH). Film samples were photoexcited using a 505 nm laser head (LDH-P-C-510, PicoQuant GmbH) pulsed at a frequency of 100 kHz, and fluence of 0.187 nJ/cm^2 . The PL was collected using a high-resolution monochromator and hybrid photomultiplier detector assembly (PMA Hybrid 40, PicoQuant GmbH).

Solid-state Nuclear Magnetic Resonance Spectroscopy:

^{19}F MAS NMR spectroscopy was performed using a Bruker 500 MHz spectrometer at 25 °C at 20 kHz. The probe was calibrated using ammonium trifluoroacetate as a standard. Powders were packed in a MAS rotor and immediately analyzed. $\text{FA}_{0.85}\text{MA}_{0.15}\text{Pb}(\text{I}_{0.85}\text{Br}_{0.15})_3$ crystals were ground using a mortar and pestle prior to immersion for 1 h at 25 °C in a 1 wt.% solution of $\text{Mo}(\text{tfd-CO}_2\text{Me})_3$ in water- and oxygen-free chlorobenzene (freeze-pump-thawed) under inert atmosphere. The dopant solution was then filtered, and the residual solvent was removed by heating for 5 min at 70 °C. Further drying of the modified perovskite powder was performed under nitrogen flow in a fumehood. Solutions of spiro-OMeTAD and $\text{Mo}(\text{tfd-CO}_2\text{Me})_3$ were blended and stirred together at 70 °C for 1 h. The solution was then dried under nitrogen and the solids scraped off the vial. A similar procedure was used to obtain powders of $\text{Mo}(\text{tfd-CO}_2\text{Me})_3$ treated with $(\text{RhCp}^*\text{Cp})_2$.

Kelvin probe measurements:

$\text{Mo}(\text{tfd-COCF}_3)_3$ and perovskites were deposited on Indium Tin Oxide (ITO) substrates in order to measure their work function by a KP Technology, SKP5050 set up. Silver was used as the reference sample to obtain the relative work function for the measuring tip. The work function of the dopant and treated perovskite samples was extracting from the difference between the tip and the samples. Data shown represents and average of 30 points per sample. The entire measurement was performed under constant nitrogen flow with both oxygen level and relative humidity levels below 10%.

The Vac-KP measurements were performed in ultra-high vacuum (UHV) with a base pressure of 10^{-9} Torr, using a standard vibrating (~ 175 Hz) gold probe. The resolution of Vac-KP is approximately 20 meV. All samples were transferred without ambient exposure from a N_2 -filled

glovebox into UHV and initially kept in the dark for 1 hour to minimize the impact of light. The WF of the gold probe was calibrated promptly after each measurement using a vacuum-peeled highly ordered pyrolytic graphite sample (HOPG, Mosaic spread value of $0.8 \pm 0.2^\circ$, NanoAndMore), with a consistent WF of 4.60 ± 0.05 eV in vacuum, as verified via UPS.

Dark Microwave Conductivity:

Microwave conductivity measurements were performed as previously described in detail,⁸ but a brief description is supplied here for completeness. An optimal TE₁₀₂ microwave cavity composed entirely of copper was fabricated according to our previous design,⁸ giving a quality factor of ~ 850 at a resonance frequency of 9.91 GHz. Our measurement consists of recording the microwave power reflection coefficient as a function of frequency about the resonance and fitting the data with a Lorentzian function. The change in Lorentzian fit parameters before and after sample introduction or doping treatment is then used to obtain the change in conductance/conductivity. COMSOL Multiphysics is used to simulate the resonance characteristics of this cavity as a function of sample conductance, generating a lookup table of Lorentzian fit parameters suitable for fitting the simulation results to experimental data. The fitting result is the absolute effective conductance of the sample.

UPS and XPS measurements:

UPS and XPS measurements were carried out in an UHV chamber with a base pressure of $< 2 \times 10^{-10}$ Torr. Samples were prepared in nitrogen glovebox and transferred under nitrogen directly to UHV without air exposure. UPS was performed with both the He I (21.22 eV) and He II (40.81 eV) photon lines. For each UPS spectrum, the satellite lines of the He discharge lamp were

carefully subtracted. XPS was performed with non-monochromatized Al K α X-rays (1486.70 eV). The overall resolutions in UPS He I, UPS He II, and XPS are 0.15 eV, 0.25 eV, and 0.80 eV, respectively. The Fermi level reference for both UPS and XPS were determined with a clean Au surface.

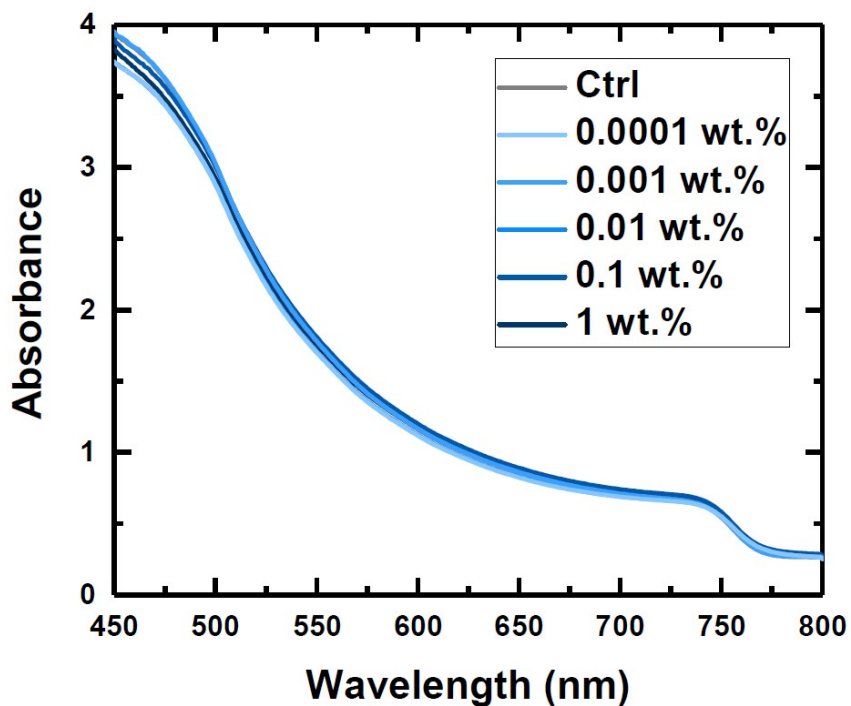


Figure S1. Absorption spectra of neat and Mo(tfd-COCF₃)₃ treated FA_{0.85}MA_{0.15}Pb(I_{0.85}Br_{0.15})₃ perovskite films.

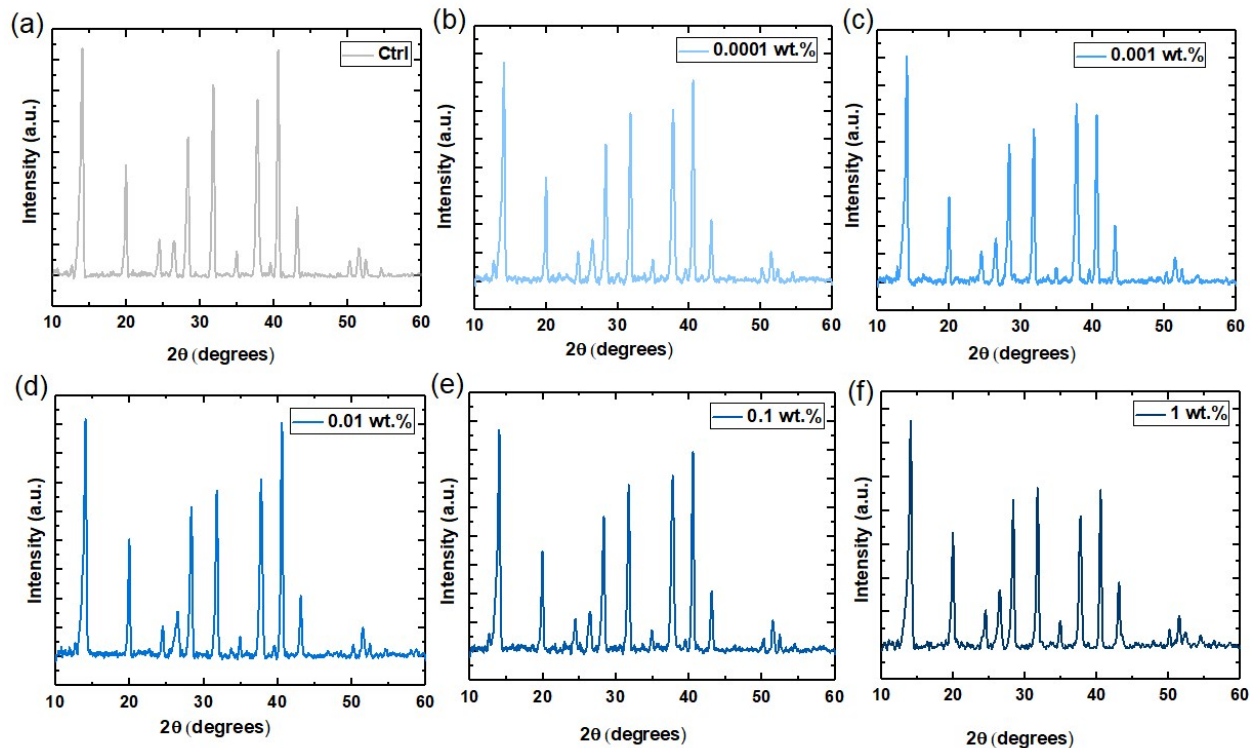


Figure S2. X-ray diffractograms of neat and $\text{Mo}(\text{tfd-COCF}_3)_3$ treated $\text{FA}_{0.85}\text{MA}_{0.15}\text{Pb}(\text{I}_{0.85}\text{Br}_{0.15})_3$ perovskite films.

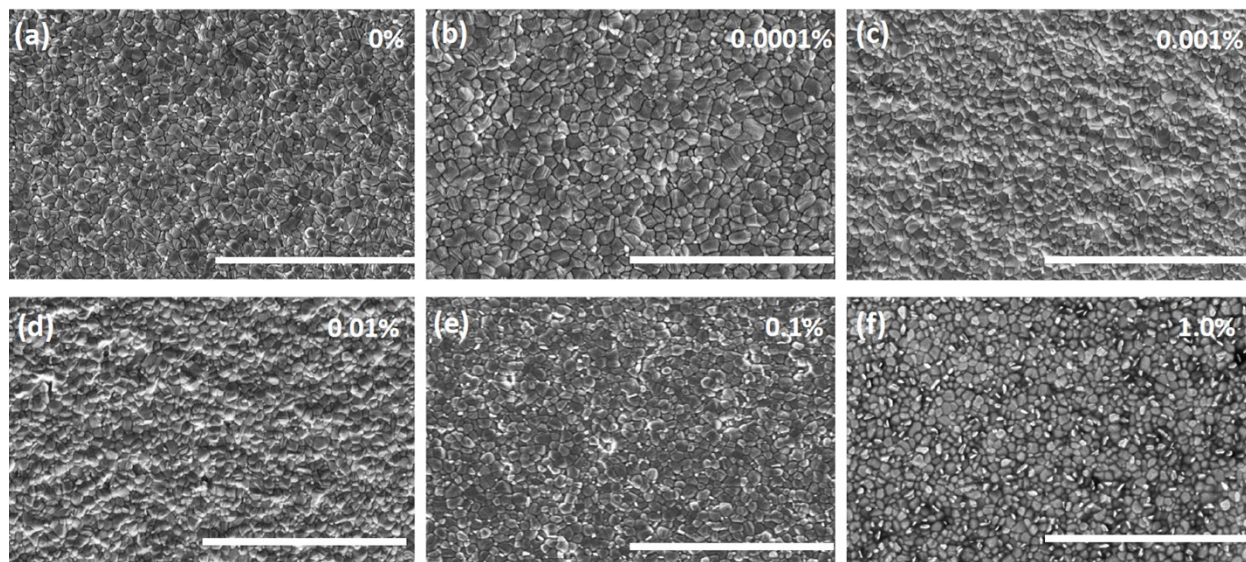


Figure S3. Microscope Images. Top view scanning electron microscope (SEM) images of (a) neat and (b)-(f) $\text{Mo}(\text{tfd-COCF}_3)_3$ (0 wt.% -1.0 wt.%) treated films. All scale bars correspond to 5 μm .

Sample	Concentration (wt.%)	W.F. (eV)	\Delta W.F. (meV)
ITO/Mo(tfd-COCF) ₃	-	-5.44 ± 0.002	-
FA _{0.85} MA _{0.15} Pb(I _{0.85} Br _{0.15}) ₃	0%	-4.62 ± 0.002	-
	0.0001%	-4.94 ± 0.045	320
FA _{0.85} MA _{0.15} Pb(I _{0.85} Br _{0.15}) ₃	0.001%	-4.99 ± 0.006	370
treated with Mo(tfd-COCF) ₃	0.01%	-5.06 ± 0.005	440
	0.1%	-5.09 ± 0.004	470
	1.0%	-5.12 ± 0.003	500

Table S1: Work function values for a neat FA_{0.85}MA_{0.15}Pb(I_{0.85}Br_{0.15})₃ perovskite sample, and samples treated with specified concentrations of Mo(tfd-COCF)₃.

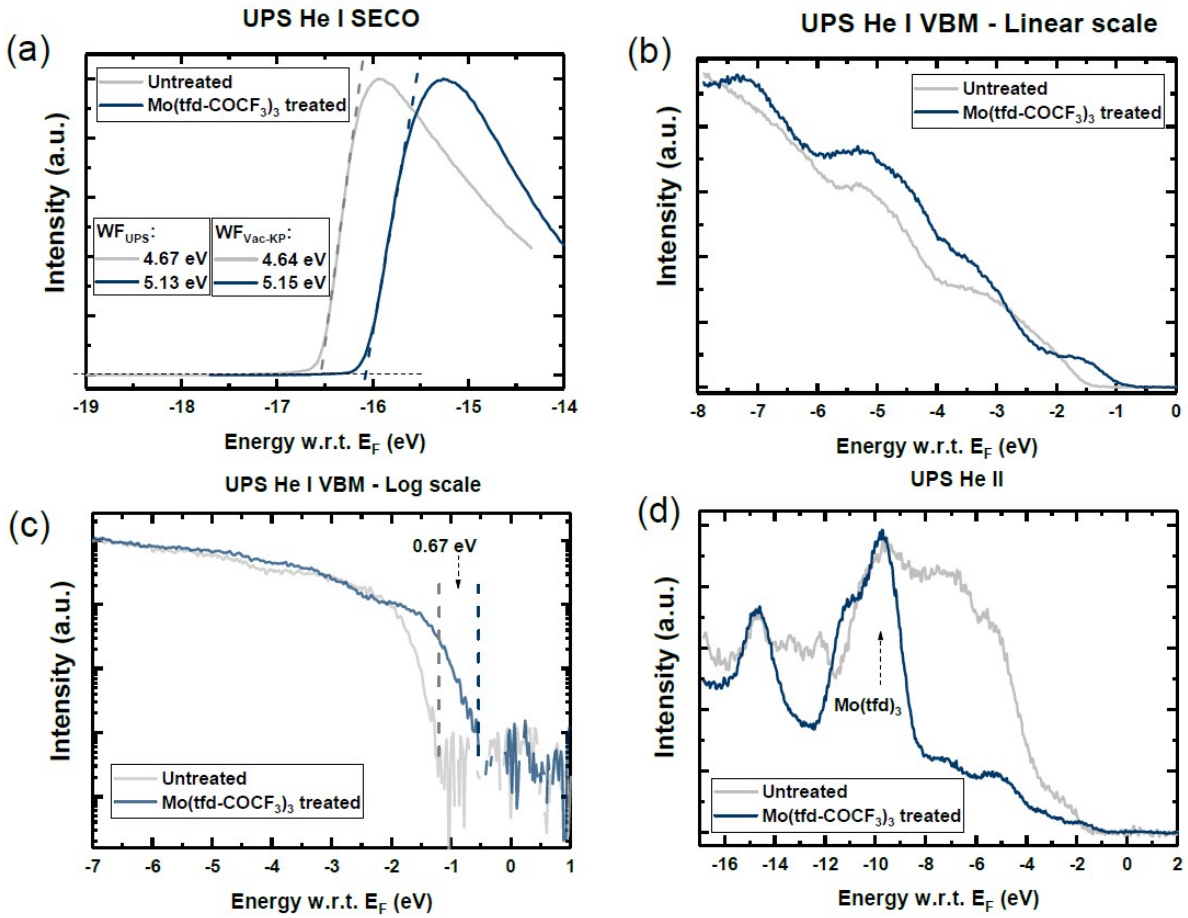


Figure S4: UPS spectra of an $\text{FA}_{0.85}\text{MA}_{0.85}\text{Pb}(\text{I}_{0.85}\text{Br}_{0.15})_3$ thin film surfaced doped with 0.1 wt% $\text{Mo}(\text{tfd}-\text{COCF}_3)_3$. (a) photoemission cut-off in UPS He I, valence-band region in UPS He I in linear scale (b) and logarithmic scale (c), and (d) valence-band region in UPS He II.

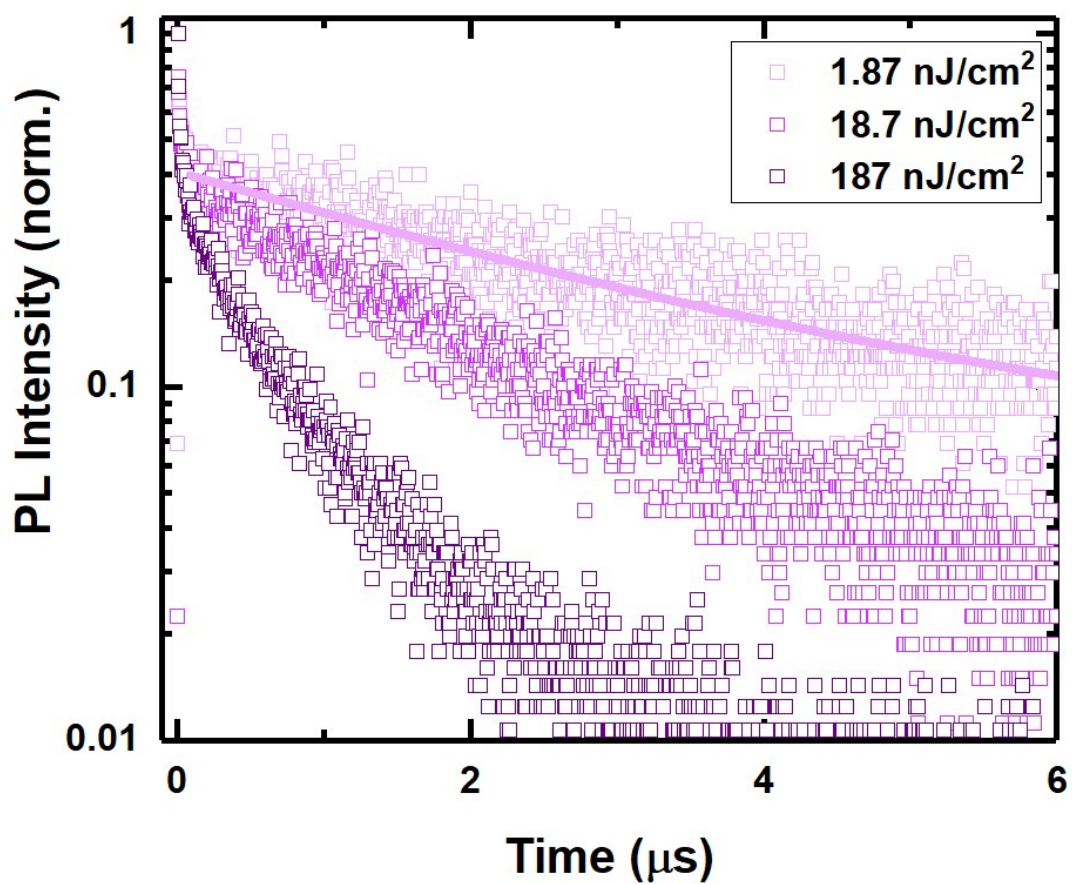


Figure S5. Fluence dependence of time-resolved photoluminescence showing the increase of bimolecular recombination with increasing intensity.

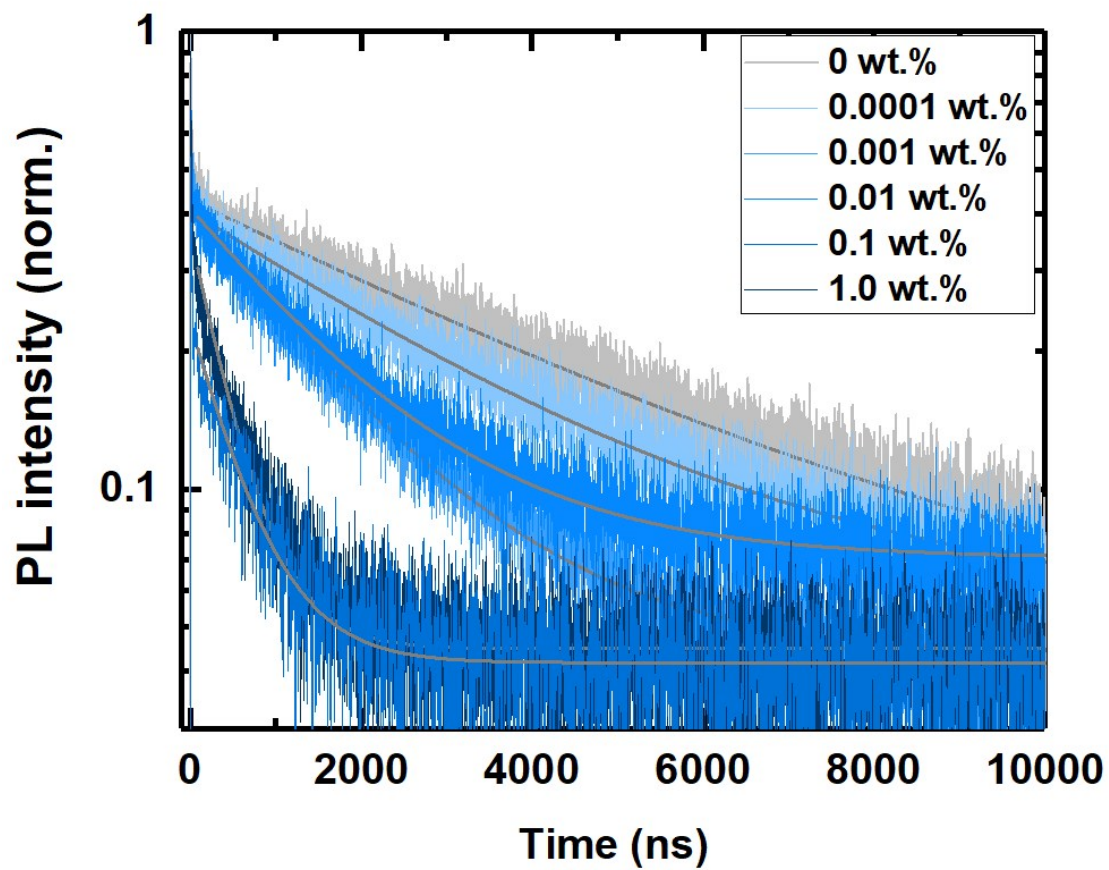


Figure S6. Time-resolved photoluminescence decays of neat and Mo-treated perovskite films. Fits are shown with solid dark grey lines.

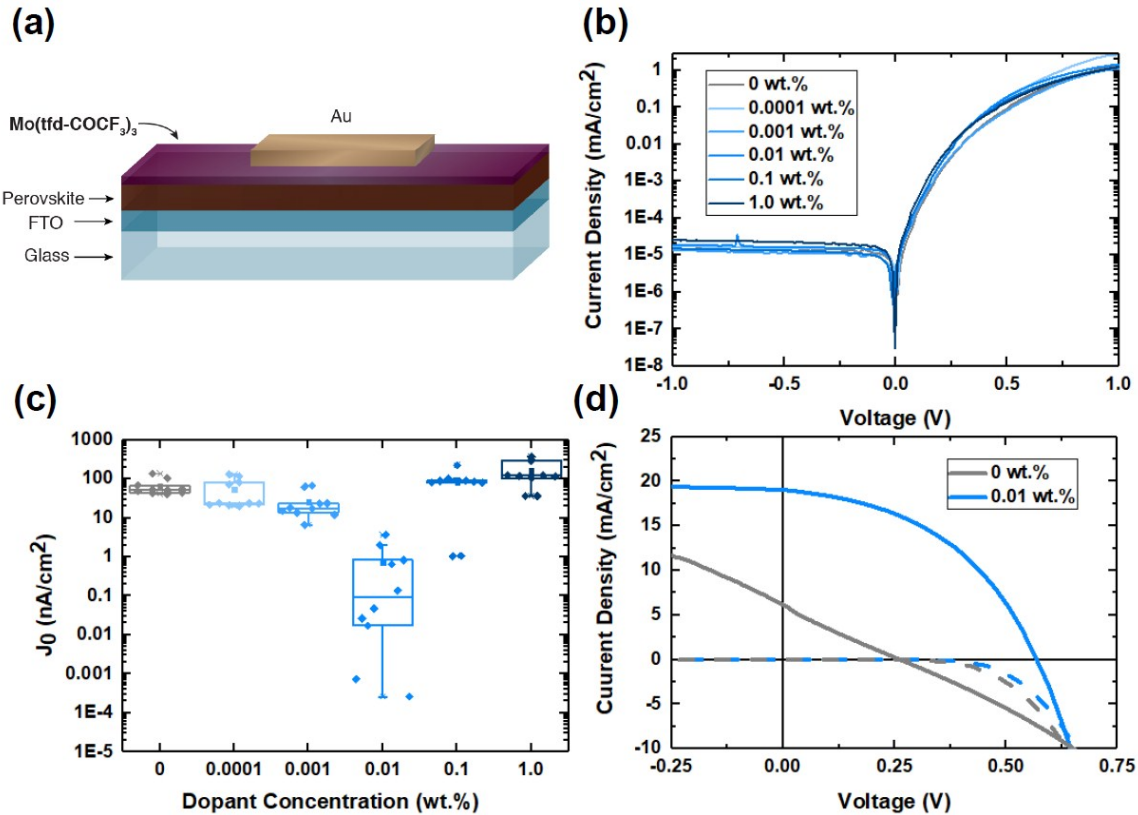


Figure S7. Dark current density-voltage (J - V) characteristics of perovskite devices without charge-selective contacts. (a) Schematic of perovskite device fabricated without charge-selective contacts. (b) Dark J - V characteristics of control and $\text{Mo}(\text{tfd-COCF}_3)_3$ -treated devices. (c) Dependence of the reverse saturation current, J_0 , on the concentration of $\text{Mo}(\text{tfd-COCF}_3)_3$ used to treat the perovskite surface. (d) Representative J - V curves (in the dark and under illumination) of a control and $\text{Mo}(\text{tfd-COCF}_3)_3$ treated device.

Figure S6d shows representative JV curves, in the dark and under illumination, of both a control device, and a device treated with a 0.01 wt.% solution of $\text{Mo}(\text{tfd-COCF}_3)_3$. We note that none of the devices were subjected to pre-biasing in these experiments. From Fig. S6d, we observe that under illumination, the device fabricated from the $\text{Mo}(\text{tfd-COCF}_3)_3$ -treated perovskite shows

significantly improved rectification. This improvement in the diode behaviour is consistent with the notion that the dopant treatment introduces an energetic asymmetry, in the form of a homojunction near the perovskite-gold interface, which enables selective charge extraction in the treated devices.

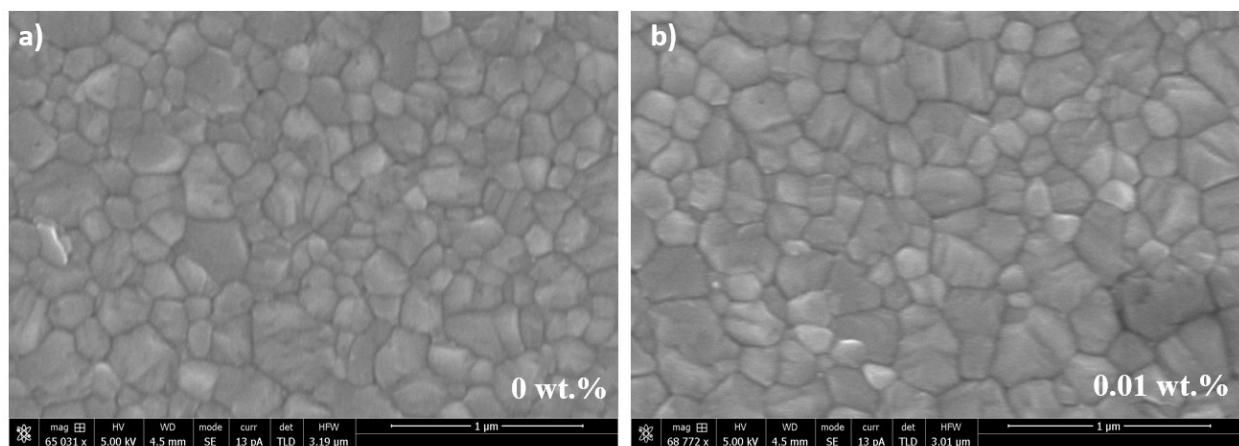


Figure S8. Microscope Images. High magnification scanning electron microscope images of (a) neat and (b) 0.01 wt.% dopant-treated perovskite films, used for device fabrication.

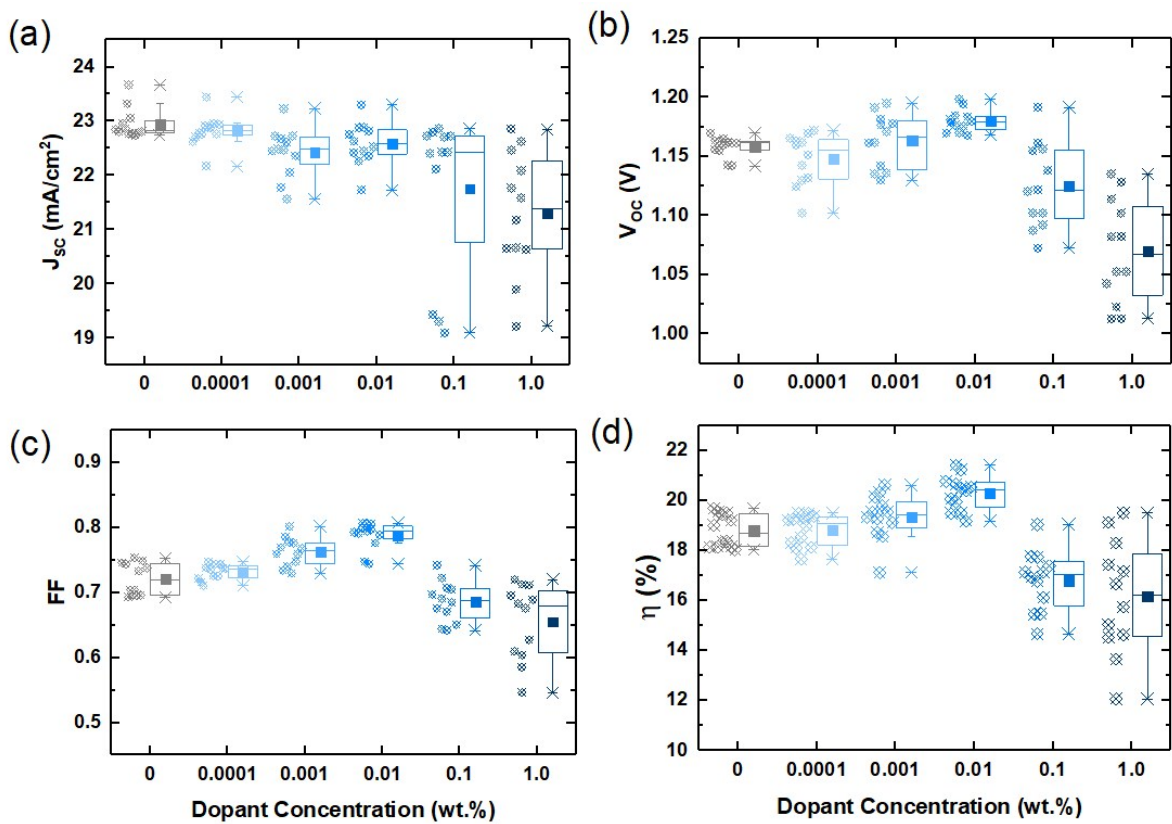


Figure S9. Performance parameters of a batch of solar cells fabricated from perovskite films, both untreated, and treated with specified dilutions of $\text{Mo}(\text{tfd-COCF}_3)_3$ in chlorobenzene. Statistics were collected for a total of 20 devices over 4 device batches.

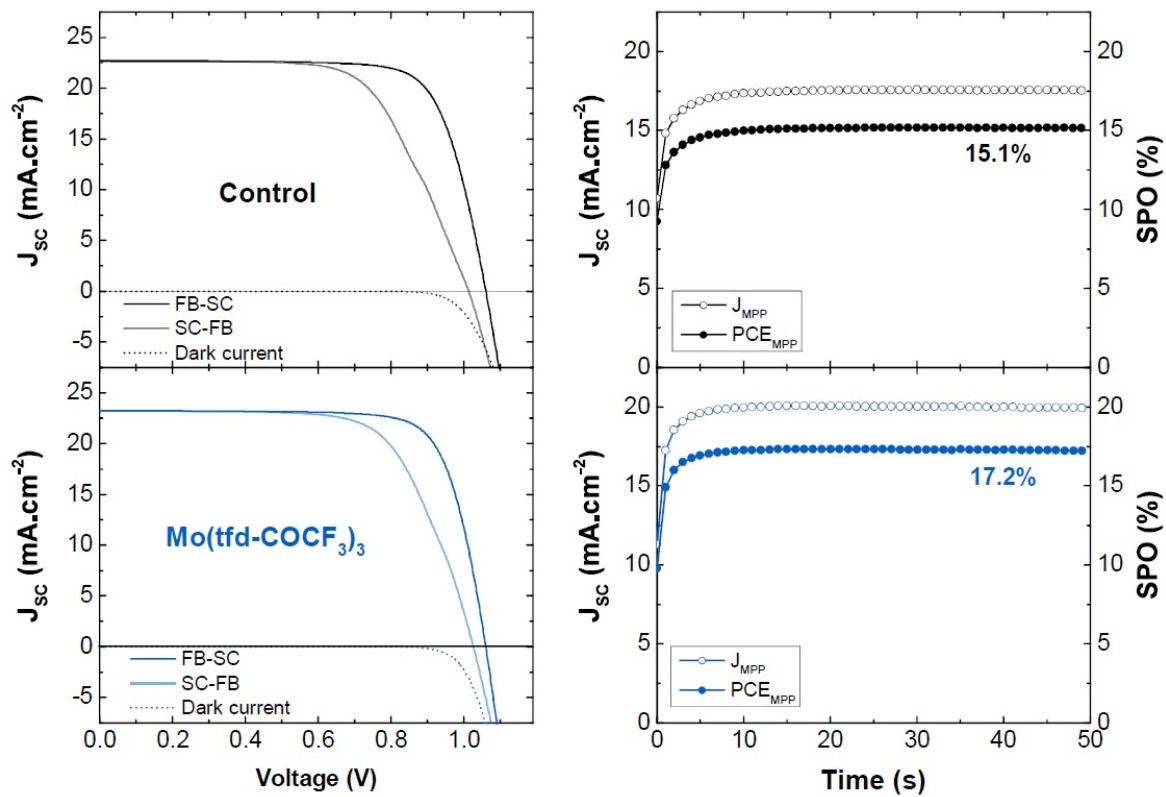


Figure S10. Current-voltage characteristics of *t*BP-free devices fabricated using spiro-OMeTAD pre-oxidised with spiro-OMeTAD²⁺.

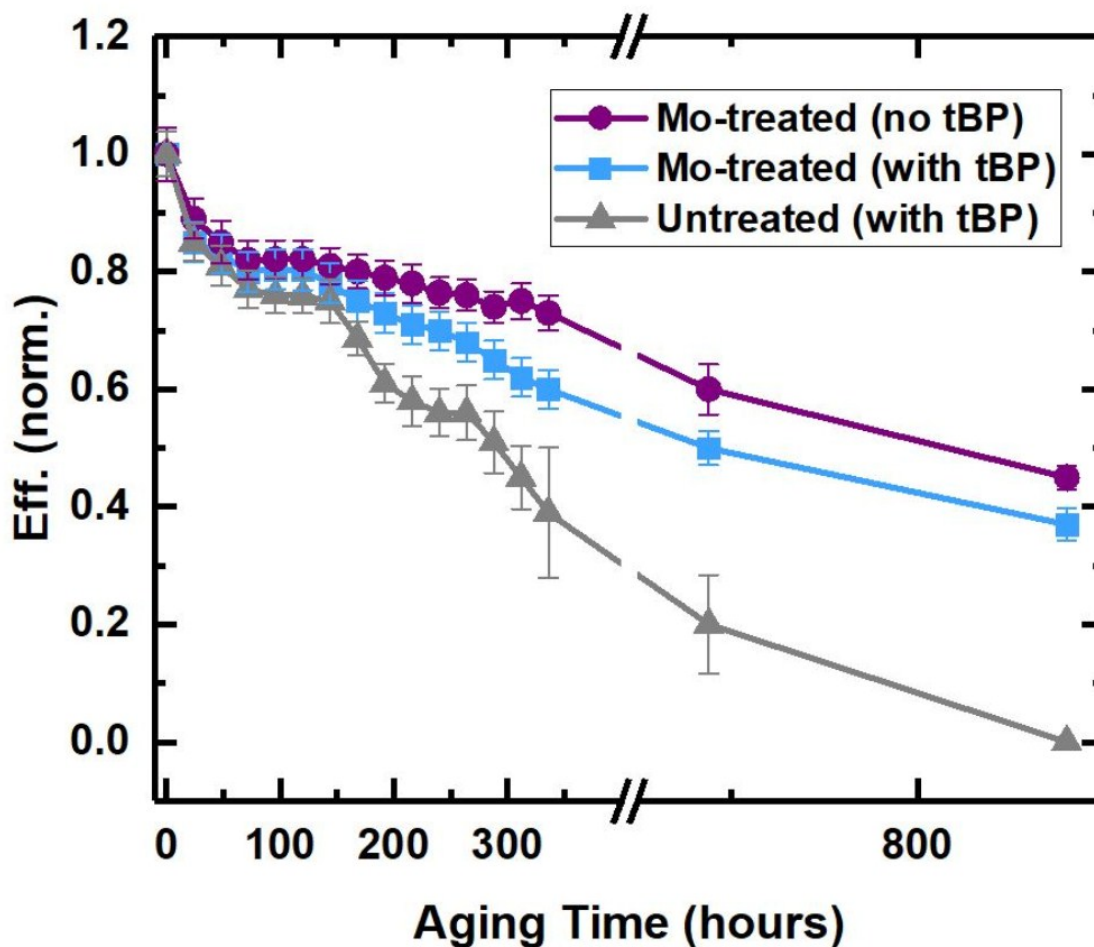


Figure S11. Thermal aging of $\text{FA}_{0.85}\text{MA}_{0.15}\text{Pb}(\text{I}_{0.85}\text{Br}_{0.15})_3$ photovoltaic devices over 840 h. Devices were aged at 85 °C in the dark, under 45% relative humidity and tested under AM 1.5 illumination at specified time intervals. Values are averaged over 20 devices per parameter.

References:

- 1 A. Dai, Y. Zhou, A. L. Shu, S. K. Mohapatra, H. Wang, C. Fuentes-Hernandez, Y. Zhang, S. Barlow, Y.-L. Loo, S. R. Marder, B. Kippelen and A. Kahn, *Adv. Funct. Mater.*, 2013, **24**, 2197–2204.
- 2 S. A. Paniagua, J. Baltazar, H. Sojoudi, S. K. Mohapatra, S. Zhang, C. L. Henderson, S. Graham, S. Barlow and S. R. Marder, *Mater. Horizons*, 2014, **1**, 111–115.
- 3 W. H. Nguyen, C. D. Bailie, E. L. Unger and M. D. McGehee, *J. Am. Chem. Soc.*, 2014,

136, 10996–11001.

- 4 S. N. Habisreutinger, B. Wenger, H. J. Snaith and R. J. Nicholas, *ACS Energy Lett.*, 2017, **2**, 622–628.
- 5 A. Pellaroque, N. K. Noel, S. N. Habisreutinger, Y. Zhang, S. Barlow, S. R. Marder and H. J. Snaith, *ACS Energy Lett.*, 2017, **2**, 2044–2050.
- 6 N. K. Noel, M. Congiu, A. J. Ramadan, S. Fearn, D. P. McMeekin, J. B. Patel, M. B. Johnston, B. Wenger and H. J. Snaith, *Joule*, 2018, **1**, 328–343.
- 7 E. H. Anaraki, A. Kermanpur, L. Steier, K. Domanski, T. Matsui, W. Tress, M. Saliba, A. Abate, M. Gratzel, A. Hagfeldt and J.-P. Correa-Baena, *Energy Environ. Sci.*, 2016, **9**, 3128–3134.
- 8 O. G. Reid, D. T. Moore, Z. Li, D. Zhao, Y. Yan, K. Zhu and G. Rumbles, *J. Phys. D. Appl. Phys.*, 2017, **50**, 493002.